POLITECNICO
MILANO 1863

SCUOLA DI INGEGNERIA INDUSTRIALE
E DELL'INFORMAZIONE

Report Assignment 5: Final Assignment

Computational Techniques for Thermochemical Propulsion

Students:

Luca Piomboni, 11011639

Riccardo Ferraresi, 10764253

Matteo Villa, 10718017

Academic year:
2024-2025

Lecturers:
Prof. Federico Piscaglia, Prof. Federico Ghioldi

Abstract

This project presents a three-dimensional simulation of a combustor operating with n-Heptane fuel injected as Lagrangian particles. Building on the configuration established in previous assignments, the study involves both a precursor cold-flow simulation and a subsequent combustion run. The cold-flow phase initializes the velocity and temperature fields without fuel injection, while the hot run includes spray injection and combustion using a one-step chemical mechanism. Numerical and physical convergence over time are carefully assessed, with particular attention paid to unsteady flow behaviours. Post-processing focuses on efficient data management and meaningful physical interpretation, including the visualization of key flow features and iso-surfaces at stoichiometric air/fuel ratio for selected time steps (0.02 s, 0.05 s, 0.08 s), and the evolution of patch-averaged pressure and temperature at inlet and outlet boundaries over time. The simulation adheres to mesh limitations and demonstrates the practical integration of CFD skills in analysing reactive flow systems.

Contents

1 Introduction **3**

2 Geometry and numerical grid **3**

3 Simulation Setup **5**
3.1 Cold Simulation Setup 5
3.2 Hot Simulation Setup 6

4 Results **6**
4.1 Precursor run 6
4.2 Combustion simulation 7
4.2.1 Velocity field 8
4.2.2 Temperature and air-to-fuel ratio 9
4.2.3 Average fields at inlet and outlet patches over time 10

5 Conclusions **11**

1. Introduction

This final assignment presents a three-dimensional simulation of a reactive, compressible flow through an aeronautical combustor using OpenFOAM. The case builds directly on the setup developed in the previous assignments but extends the domain from two to three dimensions, significantly increasing the geometrical and computational complexity.
The simulation models the injection and combustion of Heptane (C_7H_{16}), introduced in the domain as a liquid spray and tracked using Lagrangian Particle Tracking (LPT) approach. The gas-phase flow is resolved using a compressible, unsteady solver (PIMPLE), coupled with a finite-rate chemistry model, where the chemical kinetics are solved using ODE-based integration. To model combustion, the Partially-Stirred Reactor (PaSR) approach is employed.
The simulation is carried out in two stages:

1. A *cold* precursor run, in which air enters the combustor at a temperature of 900 K. No spray or combustion occurs at this stage as the goal is to initialize the velocity and pressure fields.
2. A reactive *hot* run, where spray injection and combustion are activated, using the final state of the *cold* run as the initial condition.

2. Geometry and numerical grid

The geometry under examination is a 3D aeronautical combustion chamber, cylindrically shaped, and aligned with the y axis. It is characterized by a length $l = 800$ mm and diameter $d = 240$ mm with a splitter inside, whose arrow shape has the aim of enhancing the mixing between fuel and oxidizer, thus improving combustion.

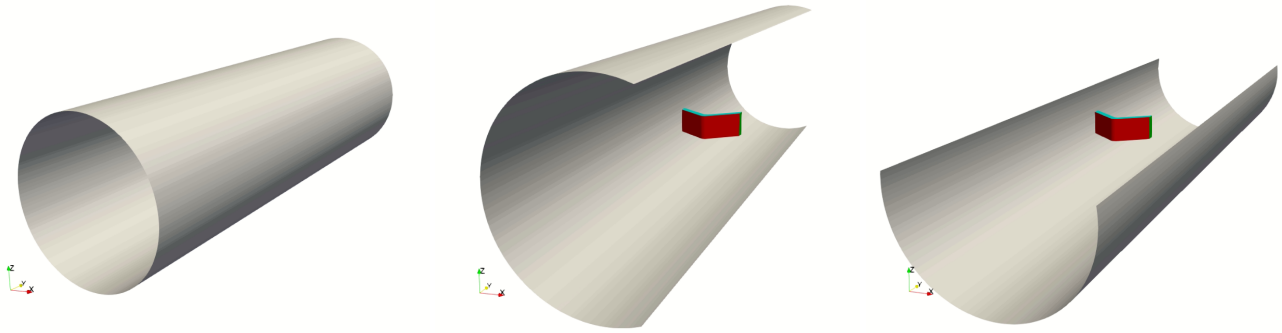

(a) Full geometry. (b) Geometry cut (X-normal plane). (c) Geometry cut (Z-normal plane).

Figure 1: Combustor geometry.

As in the previous assignments, the computational domain is bounded by an `inlet` patch, an `outlet` patch, and the `outerWalls` that represent the cylindrical walls of the combustor. Due to the three-dimensional nature of the current geometry, the splitter is now described using six distinct wall boundaries: `splitterFront`, `splitterRear`, `splitterRight`, `splitterLeft`, `splitterTop`, and `splitterBottom`.
The mesh used to discretize the geometry, shown in Figure 2, consists of approximately 380,000 polyhedral cells, in accordance with the assignment limitations. To accurately capture the flow behaviour in regions where strong gradients are present, local mesh refinements have been applied to the central core of the domain and in proximity of the splitter surfaces. These refinements enhance the resolution of boundary layers present on the wall boundaries and improve the accuracy of the interaction between the Eulerian carrier fluid and the Lagrangian spray.

The complete meshing workflow leading to the final grid consists of the following steps:

1. extraction of the surface features from the `stl` file located in the `constant` folder;
2. `blockMesh` utility, to generate the background mesh;
3. `snappyHexMesh` utility, to perform the mesh refinement;
4. `renumberMesh` utility, to renumber the cell list, thus use less memory, improve matrix conditioning and enhance solver performance.

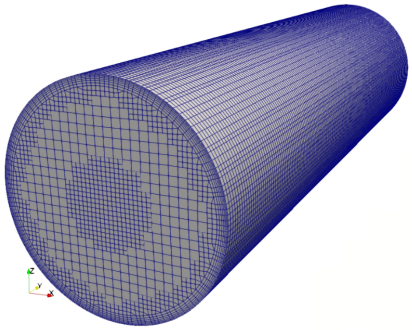

(a) External surface mesh.

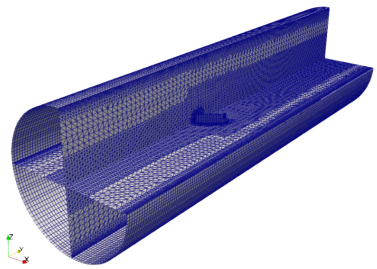

(b) Internal mesh.

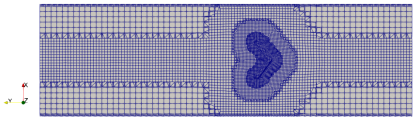

(c) Mesh cut (Z-normal plane).

Figure 2: Combustor mesh.

Finally, in order to ensure mesh suitability for accurate and stable simulation of compressible, reactive flows, the quality report generated by the `checkMesh` utility has been analyzed. Table 1 reports the most important geometric metrics for the current mesh.

Criteria	Maximum values
Non-orthogonality	64.9631
Skewness	0.822285
Aspect Ratio	6.34781
Cell Openness	3.58499e-16

Table 1: Mesh quality.

Features	Final Mesh
Number of faces	1191366
Number of cells	386983
Hexahedra	361310
Prisms	11624
Polyhedra	14049
Average non-orthogonality	7.72537

Table 2: Mesh characteristics.

All reported values lie within standard best-practice thresholds for industrial CFD, indicating that the mesh is suitable for this simulation. In particular, non-orthogonality remains below the commonly accepted upper limit (75°), skewness is low, and the aspect ratio is well-controlled across refined regions. As such, the mesh is considered appropriate for resolving both the Eulerian gas-phase field and the Lagrangian spray dynamics. The main characteristic of the employed grid are therefore summarized in Table 2.
Finally, to accurately resolve the boundary layer, a hexahedral mesh was employed. Seven prism layers were applied along the wall of the cylindrical combustion chamber, and three layers were applied along the splitter, with an expansion ratio of 1.2. The first layer thickness was set to 8×10^{-4}, ensuring appropriate near-wall resolution. This setup allowed for maintaining a suitable non-dimensional wall distance (y^+) to correctly apply the κ-ε wall function for turbulence modeling.
Figure 3 presents the behavior of y^+ throughout the combustion simulation.

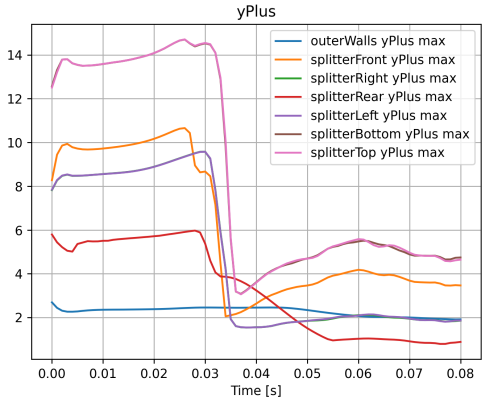

(a) Maximum y^+ on each wall patch over time.

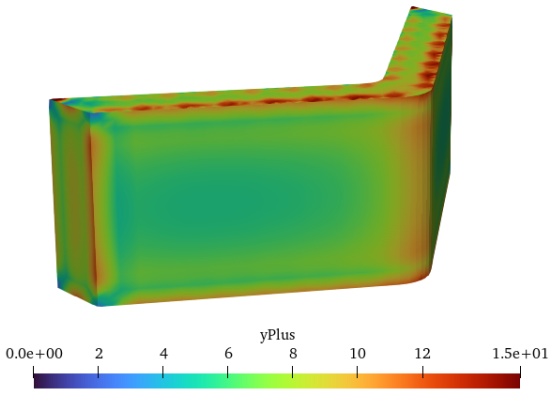

(b) Detail of y^+ on the splitter at $t = 0.02$ s.

Figure 3: Evolution and distribution of y^+ during the simulation.

As shown in Figure 3a, the splitter exhibits a sudden change in y^+ around $t = 0.035$ s. This is due to the arrival of the combusting C_7H_{16} to the splitter region, which induces sharp variations in the velocity gradients, but also changes the fluid kinematic viscosity ν. As a result, the value of y^+, defined as:

$$y^+ = \frac{yu_\tau}{\nu}, \tag{1}$$

decreases accordingly.
In contrast, the combustion chamber walls do not experience significant changes, maintaining relatively constant y^+ values throughout the simulation. Despite efforts to control wall resolution, y^+ remained below 30 due to limitations in achieving finer mesh sizes without compromising overall mesh quality.
Nevertheless, considering the nature of the simulation (a reactive, combustion-driven flow) the influence of near-wall turbulence is less dominant than in cases such as external aerodynamics. Consequently, minor inaccuracies introduced by wall treatment can be mitigated through careful tuning of combustion parameters and particle tracking models.
A final observation from Figure 3b is that the highest y^+ values are observed in regions of pronounced curvature on the splitter surface. This behaviour is attributed to the presence of stronger velocity gradients in these areas, which in turn lead to an increase in the friction velocity u_τ, and consequently, higher y^+ values.

3. Simulation Setup

The overall simulation strategy consists of an initial non-reactive precursor simulation, run for 0.05 s, during which the flow field is initialized and the high temperature at the inlet patch is convected up to the splitter section. This allows the flow to reach a stable, fully developed state before fuel injection. The final state of the precursor simulation (hereafter referred to as the *cold case*) serves as the baseline for the 3D combustor reactive simulation with particle injection, referred to as the *hot case*.
A fully compressible Finite Volume (FV) approach is used. Second-order accurate schemes in both space and time are applied for the discretization of algebraic operators in the governing equations, with flux limiters employed to handle discontinuities such as flame fronts.
The Eulerian flow solver employs the `PIMPLE` algorithm, configured as follows:

- `nOuterCorrectors` = 3
- `nCorrectors` = 2
- `nonOrthogonalCorrectors` = 2

With relaxation factors for:

- Fields: $\alpha_p = 0.3$
- Equations: $\alpha_U = 0.7$, $\alpha_k = 0.5$, $\alpha_h = 0.5$, $\alpha_\varepsilon = 0.5$

The simulations are conducted using the Reynolds-Averaged Navier–Stokes (RANS) equations with a κ–ε turbulence model. While the treatment of compressible flow and its numerical implementation has been addressed in previous assignments, this section focuses on the physical modelling specific to the present problem: the properties of n-Heptane injected and tracked via Lagrangian Particle Tracking, and the adopted combustion modelling strategy.

3.1. Cold Simulation Setup

The boundary conditions are identical for both the *cold* and *hot* simulations, as shown in Table 3.

U_{air} [m/s]	p [Pa]	T_{inlet} [K]
11	101325	900

Table 3: Boundary conditions.

The internal field temperature is initialized at 700 K. During the precursor simulation, only air is already present in the combustion chamber, and is also injected at the specified velocity. As no reactions are modelled, a maximum Courant number of 0.9 is used to allow faster time stepping, while keeping the solution stable and accurate. The simulation end time (0.05 s) provides the initial condition for the reactive hot case.

The thermo-physical properties are modelled using the JANAF (Joint Army Navy Air Force) temperature-based thermodynamics, with an energy equation based on `sensibleEnthalpy` and transport properties described by the Sutherland model.

3.2. Hot Simulation Setup

In the hot case, both combustion chemistry and particle injection are activated. This implies the adoption of a more strict condition on the maximum Courant number to handle instabilities, hence a value of 0.3 is taken as maximum. Particles of liquid heptane (C_7H_{16}) are injected into the combustion chamber using a Lagrangian spray model. The spray is introduced as a cone-shaped cloud at the centre of the inlet patch, with a total injected mass of $m = 10^{-4}$ kg over a duration of $T = 0.1$ s, following a half-sine profile. Injection is performed at a rate of 500,000 parcels per second using the `ReitzDiwakar` breakup model and a `RosinRammler` size distribution.
Spray–flow interaction is modelled via one-way coupling: the particles experience forces from the carrier gas, but the gas flow is not directly affected by the spray, except through local interactions affecting particle dynamics. For species transport and reaction, the `seulex` solver is used with an absolute tolerance of 1×10^{-8}. The only reaction modeled is the stoichiometric combustion of Heptane with Oxygen:

$$\mathrm{C_7H_{16}} + 11(\mathrm{O_2} + 3.76\ \mathrm{N_2}) \rightarrow 8\ \mathrm{H_2O} + 7\ \mathrm{CO_2} + 11 \cdot 3.76\ \mathrm{N_2} \tag{2}$$

and the stoichiometric air-to-fuel ratio is evaluated as:

$$AFR_{stoich} = \frac{\mathrm{O_2}\ +\ \mathrm{N_2}}{C_7H_{16}} = \frac{11 \cdot [(2 \cdot 16\ \mathrm{g/mol}) + 3.76 \cdot (2 \cdot 14\ \mathrm{g/mol})]}{(7 \cdot 12\ \mathrm{g/mol}) + (16 \cdot 1\ \mathrm{g/mol})} = 15.1 \tag{3}$$

As nitrogen does not participate in the reaction, it is treated as an inert species. Finally, the combustion model adopted is `PaSR` (Partially Stirred Reactor), with N_2 used as the default species for mass conservation.

4. Results

This section presents the outcomes of both the precursor and reactive simulations. All required post-processing has been performed for the specified time instances, $t = [0.02s, 0.05s, 0.08s]$, in accordance with the assignment guidelines. Additionally, further post-processing has been conducted to highlight particularly interesting results. The corresponding analyses and visualizations are discussed in the following sub-sections.

4.1. Precursor run

As already stated before, the precursor simulation aims at initializing the internal flow field for the actual combustion simulation. In Figure 4, the velocity magnitude on the XY plane, at $z = 0$, is shown. This also corresponds to the initial velocity field for the combustion simulation.

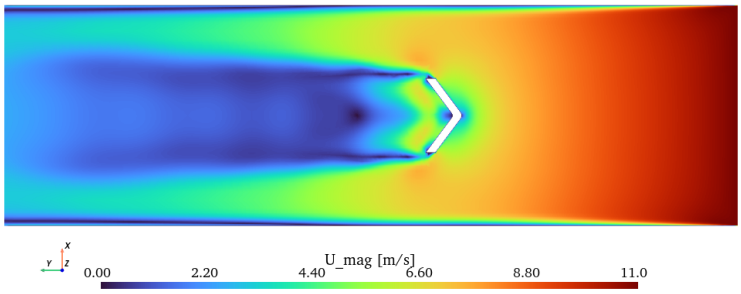

Figure 4: Velocity field on XY plane ($z = 0$).

The temperature field is also initialized through the precursor run. Starting from an internal field with uniform value equal to 700 K, the condition visible in Figure 5a is reached after 0.05 s. As desired, at the `endTime` of the run, the high temperature imposed at the inlet has reached the splitter section, where combustion will take place. Because of the temperature gradients, also large variations in density are expected, with an opposite trend. Indeed, high temperature corresponds to low density, and vice-versa (see Figure 5b).

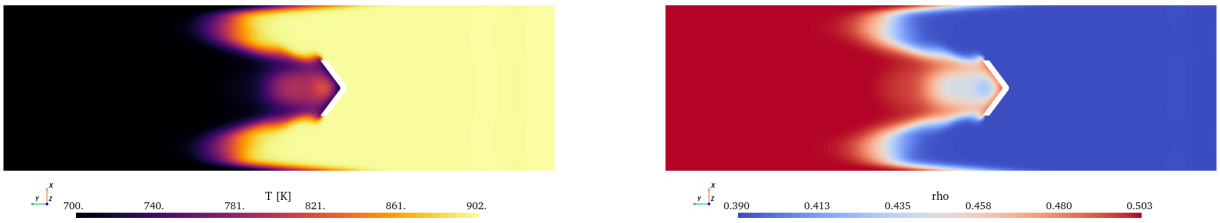

(a) Temperature field on XY plane ($z = 0$). (b) Density field on XY plane ($z = 0$).

Figure 5: Temperature and density fields on the XY plane at $z = 0$ for $t = 0.05$ s.

The stability and convergence of the precursor run is important for the convergence of the combustion simulation, too. From the visualization of the residuals (Figure 6), it is possible to observe good convergence for enthalpy, velocity, turbulent kinetic energy and its dissipation rate. Residuals on pressure are largely oscillating, and around a large value; hence, mass is not well conserved, and the coupling between pressure and velocity is not strong enough. The high oscillations can be associated to the intrinsic unsteadiness of the problem, due to the vortex-shedding induced by the presence of the splitter. Pressure residuals might be lowered by reducing the simulation time-step, or by improving the mesh. From running the `checkMesh`, it is observable a maximum non-orthogonality of around 65, which is quite large. However, the mesh is still declared `OK`, therefore it should work fine.

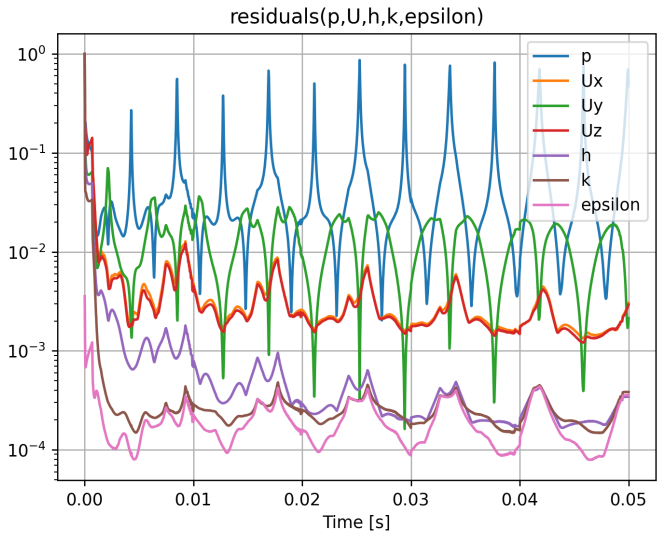

Figure 6: Residuals for the precursor simulation.

4.2. Combustion simulation

Concerning the stability of the solution, this starts already with low initial residuals because of the flow initialization performed by the precursor case. As expected, the pressure initial residuals are quite large with respect to all other physical quantities, hence there is a low coupling between pressure and velocity (see Figure 7). It is possible that employing a much finer grid would help in reducing the initial residuals on pressure, then enforcing mass conservation in a better way. Once again, periodic oscillations are present, and they are likely due to the unsteadiness of the phenomenon at hand, as already stated.

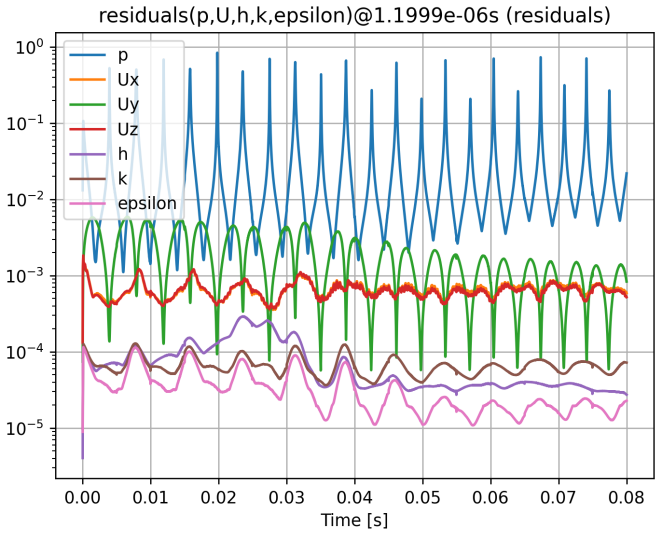

Figure 7: Residuals for the combustion simulation.

4.2.1. Velocity field

In Figure 8, the velocity magnitude field is displayed. Some main features are highlighted:

- the velocity of the sprayed particles changes across time, as the flow rate profile is a half-sine, and the maximum is reached at $t = 0.05s$;
- there is a stagnation point corresponding to the front vertex of the splitter;
- behind the splitter, a recirculating bubble appears, characterized by a very low velocity.

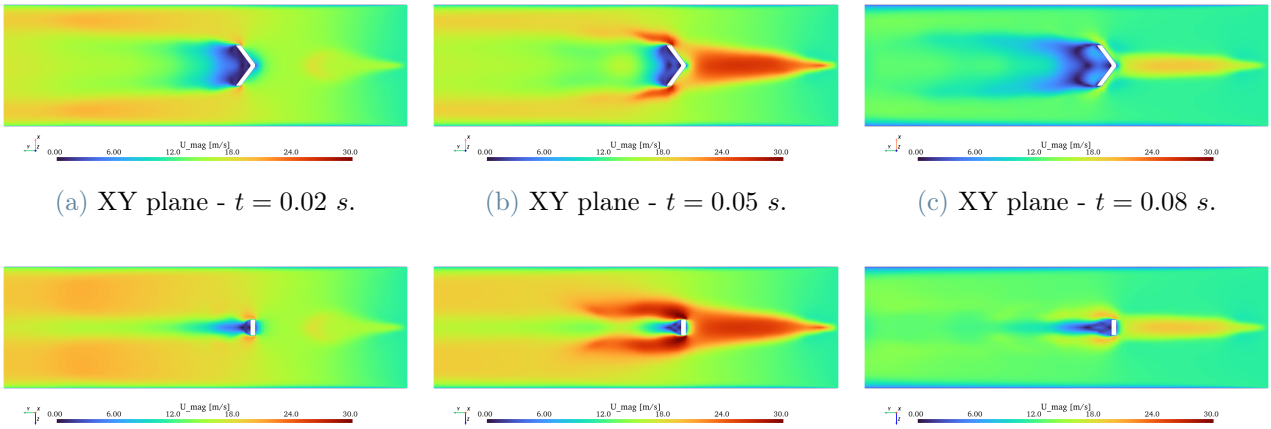

(a) XY plane - $t = 0.02$ s. (b) XY plane - $t = 0.05$ s. (c) XY plane - $t = 0.08$ s.

(d) YZ plane - $t = 0.02$ s. (e) YZ plane - $t = 0.05$ s. (f) YZ plane - $t = 0.08$ s.

Figure 8: Velocity field.

In Figure 9, the iso-surfaces for a positive value of Q-criterion are displayed. The Q-criterion is a scalar quantity used to identify rotational structures, vortices, in a flow field. It is defined as:

$$Q = \frac{1}{2}(||\Omega||^2 - ||S||^2) \tag{4}$$

where Ω is the antisymmetric part of the velocity gradient tensor, so the vorticity tensor, and S is the strain rate tensor, given by the symmetric part of the velocity gradient tensor.
A positive value of Q indicates a region of the flow that is dominated by rotation, hence it may imply the presence of a vortex core region. On the other hand, a negative Q represents areas where strain dominates over rotation, so non-vortical regions. Therefore, iso-surfaces of positive Q are used to identify vortical structures.
By observing Figure 9, it is possible to appreciate the key contribution of the splitter to combustion, by generating turbulence that enhances the mixing of species, hence limiting the amount of unburnt fuel. Fundamental

in the mixing of reactants is the spray as well. Indeed, the iso-surface of Q is visible in the zone around the spray injector, and its extension increases as the mass flow rate increases.

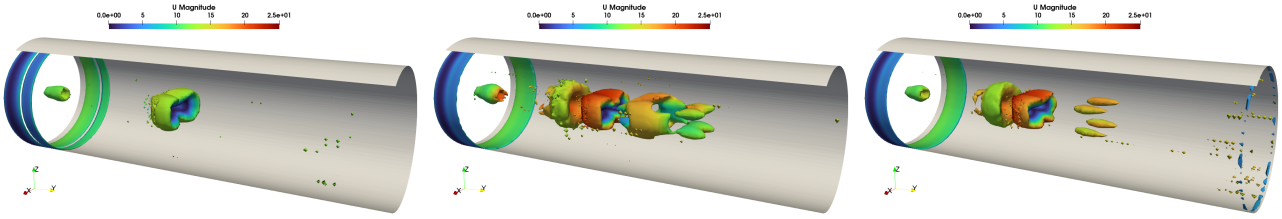

(a) $t = 0.02\ s$. (b) $t = 0.05\ s$. (c) $t = 0.08\ s$.

Figure 9: Q criterion iso-surface (Q=1200).

4.2.2. Temperature and air-to-fuel ratio

From Figure 10 it is possible to observe that the combustion reaction begins at early stages of the simulation; this is justified by the high air temperature inside the combustion chamber, around $900K$, which is much higher than the auto-ignition temperature of n-Heptane ($493.15K$). A low temperature region, instead, may be observed close to the injection point, where C_7H_{16} is sprayed inside the combustion chamber. This result is likely related to the vaporization process of the liquid fuel just after injection, to generate fuel vapor. Indeed, as one may observe in Figure 13, the central part of the spray is majorly interested by the generation of fuel vapor, and this corresponds to a lower temperature region, since the phase change occurs at constant temperature.
By looking at Figure 11 and 12, one may notice that the highest temperature is reached when the combustion occurs with the stoichiometric air-to-fuel ratio, hence with neither excess nor lack of reactants (or products). The very high temperature is due to the extremely exothermic combustion reaction.

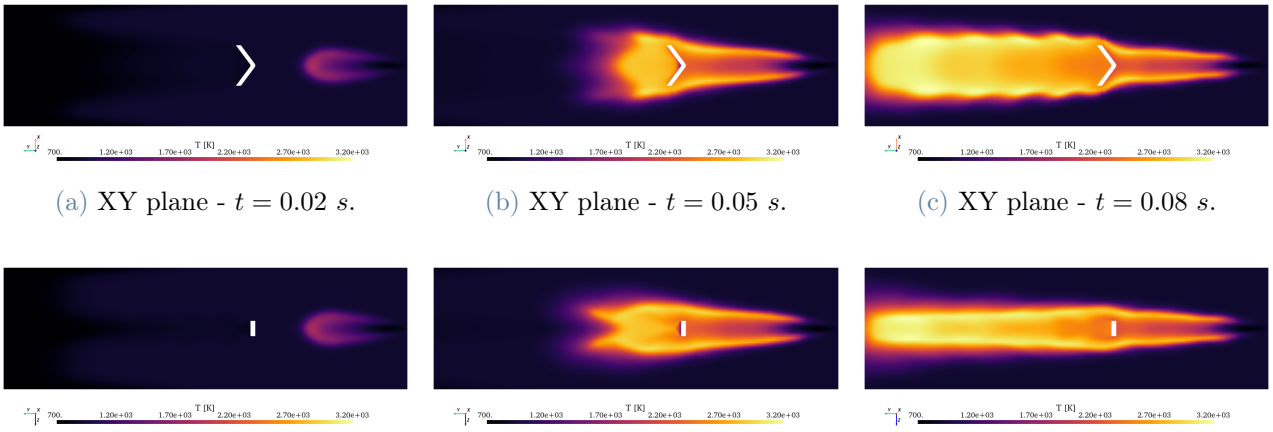

(a) XY plane - $t = 0.02\ s$. (b) XY plane - $t = 0.05\ s$. (c) XY plane - $t = 0.08\ s$.

(d) YZ plane - $t = 0.02\ s$. (e) YZ plane - $t = 0.05\ s$. (f) YZ plane - $t = 0.08\ s$.

Figure 10: Temperature field.

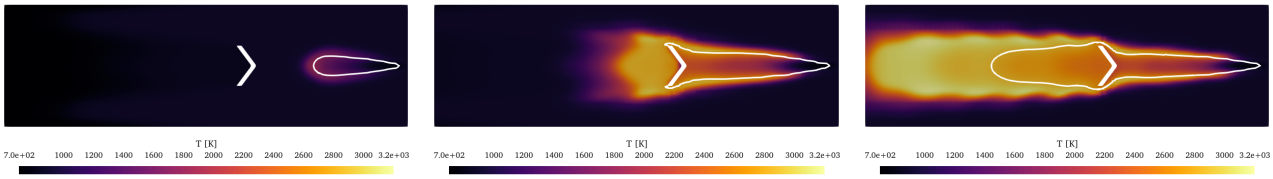

(a) XY plane - $t = 0.02\ s$. (b) XY plane - $t = 0.05\ s$. (c) XY plane - $t = 0.08\ s$.

Figure 11: Iso-lines of stoichiometric air-to-fuel ratio on XY plane.

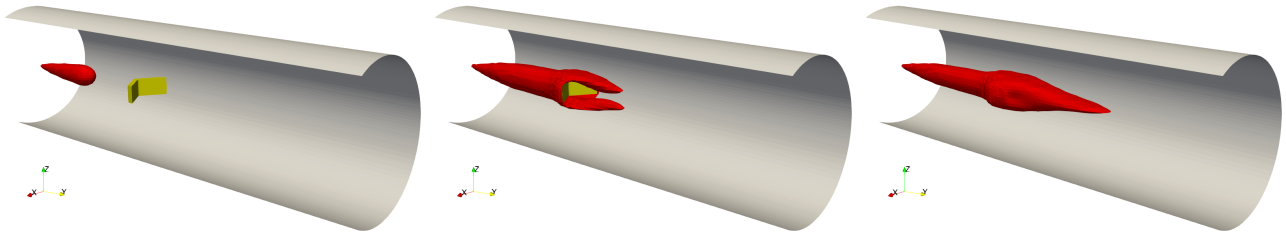

(a) $t = 0.02\ s$. (b) $t = 0.05\ s$. (c) $t = 0.08\ s$.

Figure 12: Iso-surfaces of stoichiometric air-to-fuel ratio.

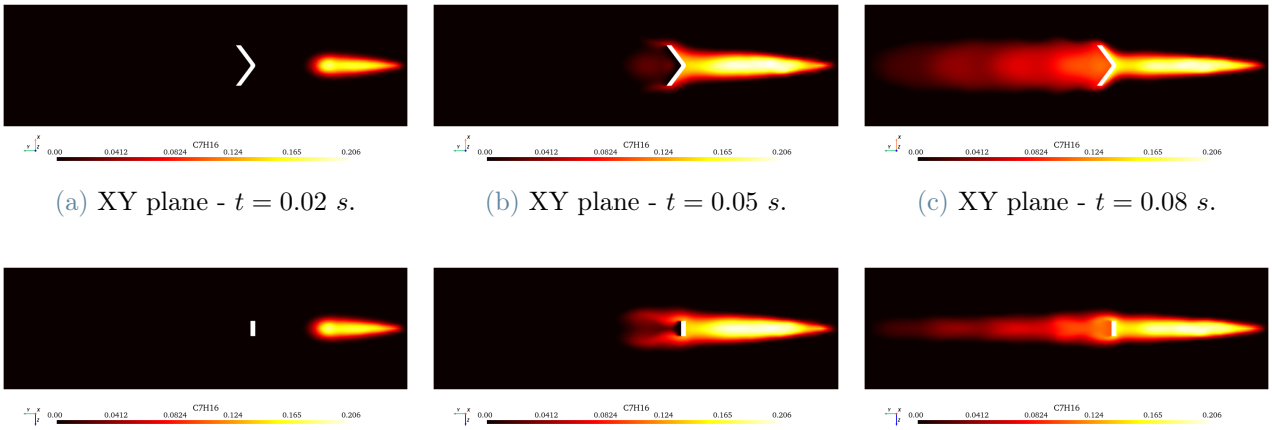

(a) XY plane - $t = 0.02\ s$. (b) XY plane - $t = 0.05\ s$. (c) XY plane - $t = 0.08\ s$.

(d) YZ plane - $t = 0.02\ s$. (e) YZ plane - $t = 0.05\ s$. (f) YZ plane - $t = 0.08\ s$.

Figure 13: Fuel vapor C_7H_{16}.

4.2.3. Average fields at inlet and outlet patches over time

Figure 14 shows the evolution in time of the average pressure on the inlet and outlet patches, respectively. The outlet pressure remains constant, due to the imposed boundary condition. As opposed to this, at the inlet the pressure is fluctuating around a constant value. This phenomenon may be related to the variations of density and velocity of the flow, and to the turbulent structures generated by the injection of fuel.

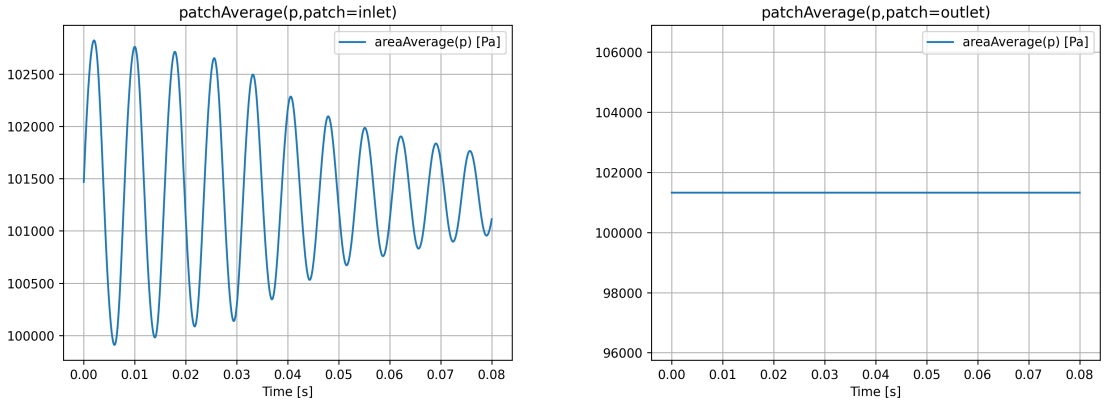

(a) Inlet. (b) Outlet.

Figure 14: Average pressure on inlet and outlet patches over time.

At the inlet section, the temperature does not evolve in time, because of the enforced `fixedValue` boundary condition.
On the other hand, at the outer section, the temperature starts from the internal field value of $T_{IF} = 700\ K$,

and is kept constant up to around $t = 0.02\ s$ as it may be verified also from the first image in Figure 10. Then, the high temperature flow reaches the outlet section and an increase in temperature at the outlet patch is observable, stabilizing around the inlet value of $T_{inlet} = 900\ K$. If no combustion was considered, then the evolution of temperature would have stopped once the whole domain had reached the value imposed at the inlet (higher limit). However, this is a combustion simulation, which involves a very exothermic reaction that generates a high temperature region behind the splitter. This region expands towards the outlet and out of the domain, producing the very steep increase in temperature that we observe in Figure 15b from around $t = 0.07\ s$ until the end of the simulation.

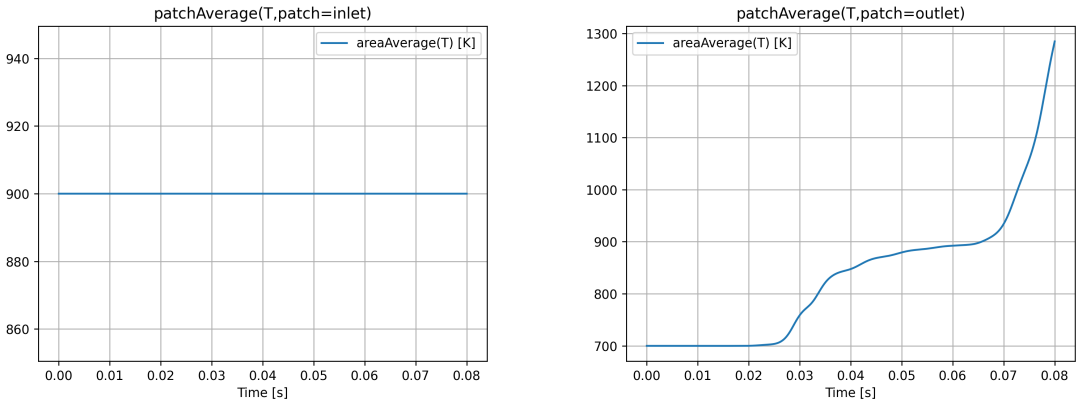

(a) Inlet.

(b) Outlet.

Figure 15: Average temperature on inlet and outlet patches over time.

5. Conclusions

This work concludes with a reflection on the key challenges and achievements of the simulation process. A fundamental aspect was the meshing strategy, which relied on the `snappyHexMesh` utility because of its capability to handle complex geometries. Despite the use of a relatively coarse mesh (approximately 380,000 cells), careful mesh refinement and geometry-conforming techniques allowed for a reasonable level of accuracy in capturing the main flow features.

The inherently multi-physics nature of the problem introduced significant computational challenges. The use of a Lagrangian spray model required continuous interaction between the liquid and gaseous phases, encompassing exchanges of momentum, mass, and heat. This added complexity particularly affected the accurate modeling of spray breakup and evaporation, both critical to initiating combustion. Therefore, the choice of appropriate submodels for these processes was essential to ensure reliable results.

A notable limitation in the modeling strategy was the exclusion of intermediate combustion products. Although a finite-rate chemistry framework supports such extensions, they were omitted to reduce computational cost and complexity. However, the selected chemical reaction mechanism proved to be sufficient to represent the dominant combustion dynamics of heptane.

The modeling of the flame as a sharp discontinuity placed further demands on spatial and temporal resolution. Ensuring numerical stability and accuracy required the use of conservative Courant numbers and small time steps, which increased the computational load. To manage this, parallelization was employed across ten cores, enabling a more efficient resolution of the governing equations.

While advanced turbulence models such as LES or DNS could provide a deeper understanding of mixing and combustion phenomena, they were not feasible within the available computational resources. Thus, a RANS-based turbulence model was adopted as a practical compromise.

In summary, despite simplifications and computational constraints, the simulation successfully captured the essential fluid dynamic and combustion behaviours of the system. The results show physically consistent trends and offer valuable insight into spray-flame interaction, validating the modeling choices adopted within the scope of the study.